Electronic Supplementary Material (ESI) for Nanoscale Advances.

Supporting Information

Metal-Organic Framework Templated Pd/CeO_2@N-doped Carbon for Low-temperature CO Oxidation

Weidong Fan,[#,a] Dongyuan Liu,[#,a] Xia Wang,[a] Xiuping Liu,[b] Dongwei Cao,[a] Lili Fan,*[a] Zhaodi Huang,[a] Wenyue Guo[a] and Daofeng Sun[a]

[a] School of Materials Science and Engineering, College of Science, China University of Petroleum (East China), Qingdao, Shandong 266580, China

[b] College of Materials Science and Engineering, Linyi University, Linyi, Shandong 276000, China

E-mail: lilifan@upc.edu.cn

[#] These authors contributed equally.

1. Crystallographic data of Pd/Ce-MOF

A suitably sized crystal was selected for structure analysis. Single crystal X-ray diffraction analysis was performed at 293 K on a Agilent Xcalibur Eos Gemini diffractometer with (Cu) X-ray Source (Cu-Kα λ = 1.54184 Å). [CCDC 18354611 contains the supplementary crystallographic data for this paper. These data can be obtained free of charge from The Cambridge Crystallographic Data Centre via www.ccdc.cam.ac.uk/data_request/cif.]

Crystal structure of Pd/Ce-MOF:

During the solvothermal reaction of 4,4'-H_2bpydc, $Pd(OAc)_2$, and $Ce(NO_3)_3 \cdot 6H_2O$ in mixed solvents of acetonitrile (CH_3CN) and H_2O (v /v = 1 :1), the Pd/Ce-MOF in a high yield (85%) is obtained. Single-crystal structure analysis reveals that the Pd/Ce-MOF belongs to the triclinic system and $P\bar{1}$ space group. As shown in Fig. S1a, its asymmetric unit includes a Ce^{3+} ion, two Pd^{2+} ions, two (4,4'-bpydc^{2-}) anions, three acetate (OAc^-) ions, one coordinated H_2O molecule, and one uncoordinated of H_2O molecule. Pd^{2+} forms a coordination bond with the nitrogen atom on the anion (4,4'-bpydc)$^{2-}$ and the oxygen atom on the acetate, respectively. The two pyridine carboxylic acid ligands (4,4'-Bpydc^{2-}) are arranged in parallel. The distance between two Pd^{2+} ions is 2.89 Å, which belongs to the weak force between Pd···Pd (d <3.5 Å). Ce^{3+} ions are nine-coordinated with six oxygen atoms from the organic ligand (4,4'-Bpydc^{2-}), one oxygen atom from the coordination of H_2O molecules, and two oxygen atoms from the acetate groups. Two adjacent Ce^{3+} ions are interconnected by the bidentate coordination of the carboxylic acid groups to form a binuclear metal center (Ce-SBU) (Fig. S1b and 1c). The binuclear metal centers are interconnected by organic ligands (4,4'-bpydc^{2-}) to form a one-dimensional structure in space, as shown in Fig. S1e. Through the intermolecular force, the chains are constructed into a three-dimensional structure (Fig. S1d).

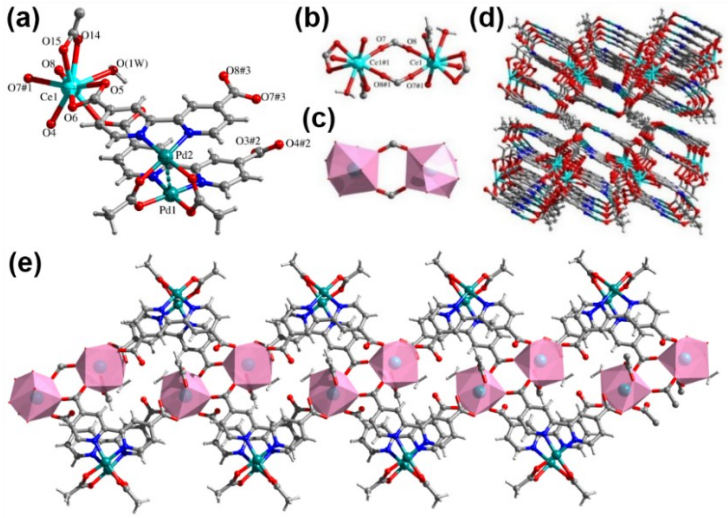

Fig. S1 (a) Asymmetric unit of Pd/Ce-MOF; (b) and (c) The double nuclear structure of Ce-SBU; (d) Stacking structure of Pd/Ce-MOF viewed from b axis; (e) 1D wavy chain structure in Pd/Ce-MOF.

Table S1. Crystal data and structure refinement of Pd/Ce-MOF.

Compound	Pd/Ce-MOF
Furmula	$C_{30}H_{26}CeN_4O_{17}Pd_2$
Formula weight	1067.47
Temperature/K	293.8(5)
Crystal system	triclinic
Space group	P-1
a/Å	10.4340(6)
b/Å	12.4622(7)
c/Å	14.1273(8)
α/deg	93.984(5)
β/deg	95.627(5)
γ/deg	114.527(5)
V/Å^3	1650.81(17)
Z	2
ρ_{calcg}/cm^3	2.148
μ/mm^{-1}	2.521
GOF	1.041
R_1[a]/wR_2[b] I> 2σ(I)	0.0355/0.0853
R_1, wR_2 (all data)	0.0453, 0.0924

[a]$R_1 = \Sigma(||F_0| - |F_c||)/\Sigma|F_0|$. [b]$wR_2 = [\Sigma w(|F_0|^2 - |F_c|^2)^2/\Sigma(F_0^2)^2]^{1/2}$

Table S2. The lengths (Å) of coordination bonds in Pd/Ce-MOF

Bond	Length/Å	Bond	Length/Å
Ce(1)-O(2)	2.425(4)	Pd(2)-O(21)$^{\#2}$	2.020(5)
Ce(1)-O(3)	2.624(4)	Pd(2)-O(32)$^{\#2}$	2.003(4)
Ce(1)-O(4)$^{\#1}$	2.389(4)	Pd(1)-O(9)	2.017(4)
Ce (1)-O(5)	2.572(4)	Pd(1)-O(10)	2.013(4)
Ce(1)-O(6)	2.621(4)	Pd(1)-N(11)$^{\#4}$	2.015(5)
Ce(1)-O(12)	2.404(4)	Pd(1)-N(12)	2.014(5)
Ce(1)-O(13)	2.507(4)	O(4)-Ce(1)$^{\#1}$	2.389(4)
Ce(1)-O(24)	2.903(5)	N(13)-Pd(2)$^{\#3}$	2.014(4)
Ce(1)-O(25)	2.586(5)	O(21)-Pd(2)$^{\#4}$	2.020(5)
Pd(2)-Pd(1)$^{\#2}$	2.8942(6)	N(11)-Pd(1)$^{\#2}$	2.015(5)
Pd(2)-N(14)	2.019(5)	O(32)-Pd(2)$^{\#4}$	2.003(4)
Pd(2)-N(13)$^{\#3}$	2.014(4)		

Symmetry Transformations used to generate equivalent atoms for Pd/Ce-MOF

$^{\#1}$ -X,1-Y, -Z; $^{\#2}$+X, -1+Y, +Z; $^{\#3}$ -X, -Y, -Z; $^{\#4}$ +X, 1+Y, +Z

2. PXRD characterization of Pd/Ce-MOF

The powder X-ray diffraction (PXRD) of the Pd/Ce-MOF was performed at room temperature. The corresponding PXRD spectrum is shown in Fig. S2. It can be seen that the peaks of the Pd/Ce-MOF match well with the simulated pattern, indicating that the Pd/Ce-MOF crystals obtained are of a high phase crystallinity and purity.

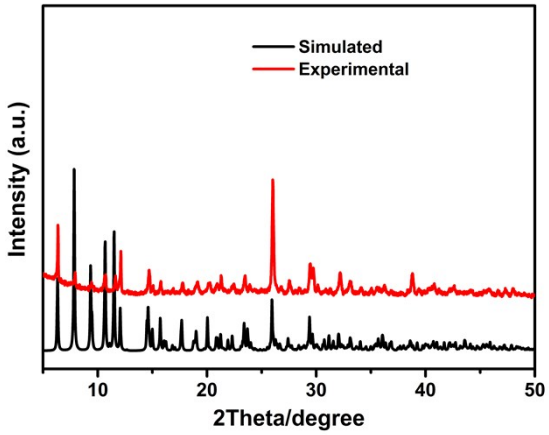

Fig. S2 The PXRD pattern of Pd/Ce-MOF (the black line is the simulated pattern and the red line is the experimental pattern).

3. FT-IR characterization of Pd/Ce-MOF

The Fourier transform infrared (FTIR) spectrum of the Pd/Ce-MOF was collected on a Nicolet 330 FTIR spectrometer by using the KBr method (Fig. S3). The main infrared absorption peaks (v/cm^{-1}) are: 3432 (s), 3054 (m), 2356 (w), 1670 (s), 1591 (s), 1540 (s), 1380 (s), 788 (s), 700 (s). The wide absorption peak of 3415 cm^{-1} belongs to the hydroxyl stretching vibration of coordination water in Pd/Ce-MOF. The characteristic absorption peak of free carboxyl group does not appear at 1720-1690 cm^{-1}, indicating that all the carboxyl groups of the 2,2'-bipyridyl-4,4'-dicarboxylic acid ligand have been deprotonated, which can be proved by peaks of 1670, 1591 and 1540 cm^{-1}. The absorption peaks of 1380 and 788 cm^{-1} can be assigned to the symmetrical vibration of carboxyl (COO^-) and the deformation vibration of pyridine ring, respectively.

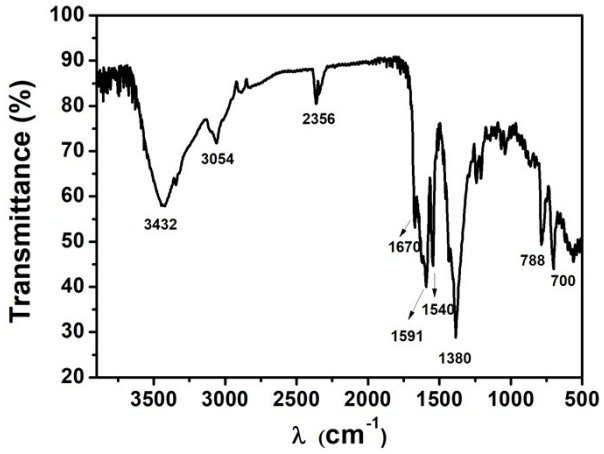

Fig. S3 FT-IR spectrum of Pd/Ce-MOF.

4. TGA characterization of Pd/Ce-MOF

TGA data was collected using the Mettler Toledo TGA/DSC-1 thermal analysis system with a heating rate of 10 ^{o}C min^{-1}. The TGA curve of Pd/Ce-MOF is shown in Fig. S4. From 40 to 170 ^{o}C, the sample slowly loses weight and the percentage of weight loss is 2.3 %. It is attributed to the removal of free solvent molecules and the coordinated water molecules in Pd/Ce-MOF structure. From 170 to 195 ^{o}C, the sample loses weight quickly and the weight loss ratio is 3.8 % due to the removal of coordinated acetate groups. From 195 to 330 ^{o}C, the mass of the sample does not change much, indicating that the Pd/Ce-MOF is basically stable to 330 ^{o}C. After 330 ^{o}C, the sample rapidly loses weight as the temperature increases, which corresponds to the collapse of the MOF backbone and the decomposition of organic ligands.

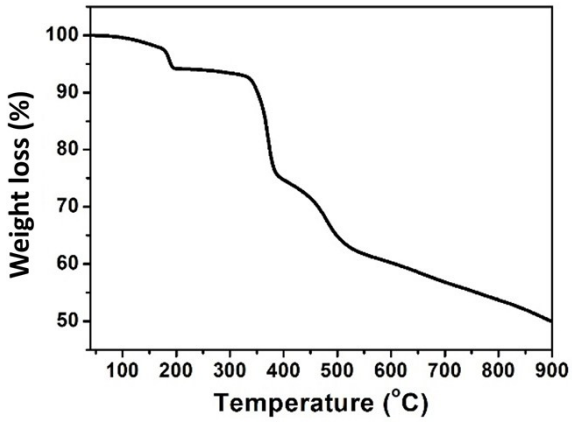

Fig. S4 TGA curve of Pd/Ce-MOF under N_2 atmosphere.

5. TEM characterization of Pd/CeO_2@NC-600 and 800

Structure details of Pd/CeO_2@NC-600 and 800 were investgated by TEM (Fig.S5). As illustrated, the Pd/CeO_2@NC-600 shows similar struture with Pd/CeO_2@NC-700 in Fig. 1, while changes can be observed for Pd/CeO_2@NC-800. No clear lattice fringes are obtained for the particle connected with Pd particle, indicating the structure transformation of CeO_2 from crystalline to amorphous, which is consistent with the XRD and XPS results.

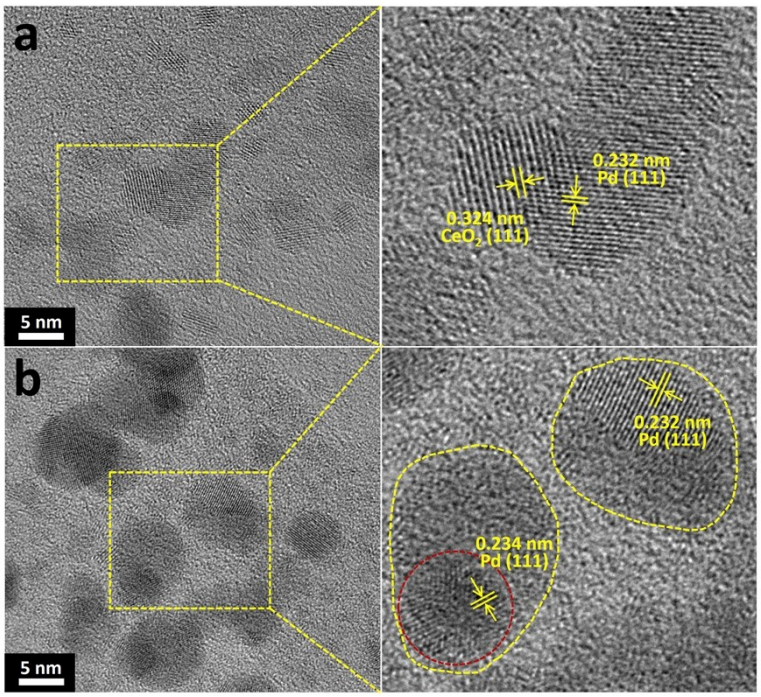

Fig. S5 TEM images of (a) Pd/CeO_2@NC-600 and (b) Pd/CeO_2@NC-800.

6. N_2 adsorption-desorption characterization of Pd/CeO_2@NC-X

The specific surface ares of MOF-derived Pd/CeO_2@NC-X nanocomposites were analyzed through the N_2 adsorption isotherms (Fig. S6), which demonstrate that all the samples present the typical type IV isotherms. The specific surface areas of the samples vary with the pyrolysis temperature. Pd/CeO_2@NC-700 has the largest surface area (about 56 m^2 g^{-1}) and pore size (13.1 nm). The isotherms of Pd/CeO_2@NC-700 show a H3 hysteresis loop, which is evidenced by the appearance of the capillary condensation step at P/P_0 = 0.75-1.0.

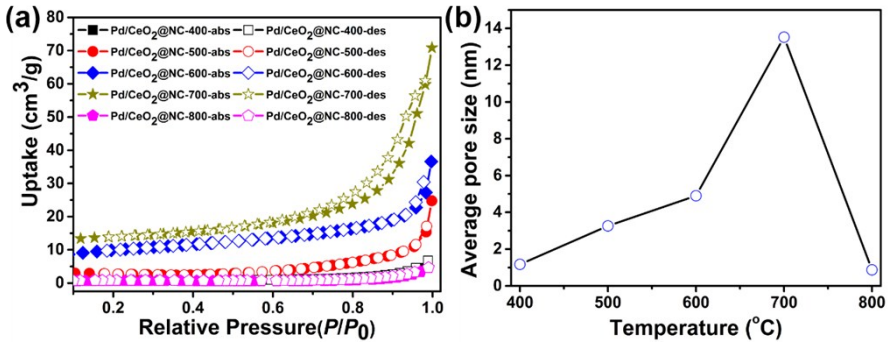

Fig. S6 (a) N_2 adsorption isotherms and (b) the average pore size distribution of the Pd/CeO_2@NC-X nanocomposites.

7. Raman characterization of Pd/CeO_2@NC-700

Raman spectrum was collected via a HORIBA Evolution Raman spectroscope using the 532 nm incident wavelength. As shown in Fig. S7, two peaks located at 1359 and 1590 cm^{-1} corresponds to the D-band and G-band, respectively. The I_D/I_G ratio (~ 0.97) and narrow G band indicate the formation of partly graphitized carbon structure, which is converted from the 4,4'-H_2bpydc ligands during pyrolysis.

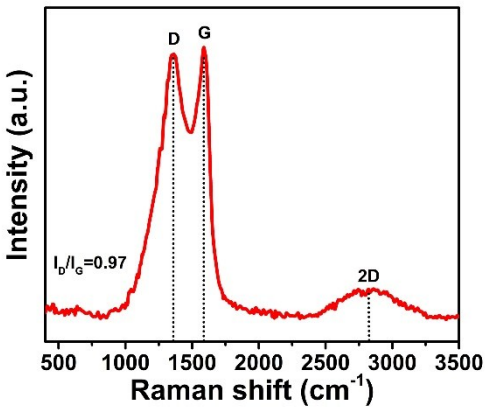

Fig. S7 Raman spectrum of the Pd/CeO_2@NC-700.

8. XPS characterization of Pd/CeO_2@NC-600 and 800

XPS spectra were recorded on an Thermo Scientific X-ray Photoelectron spectrometer (ESCA250Xi) to provide insights into the detailed chemical composition and bonding configuration of the Pd/CeO_2@NC-600 and 800. The results are summerized in Fig.S8 and Fig.S9.

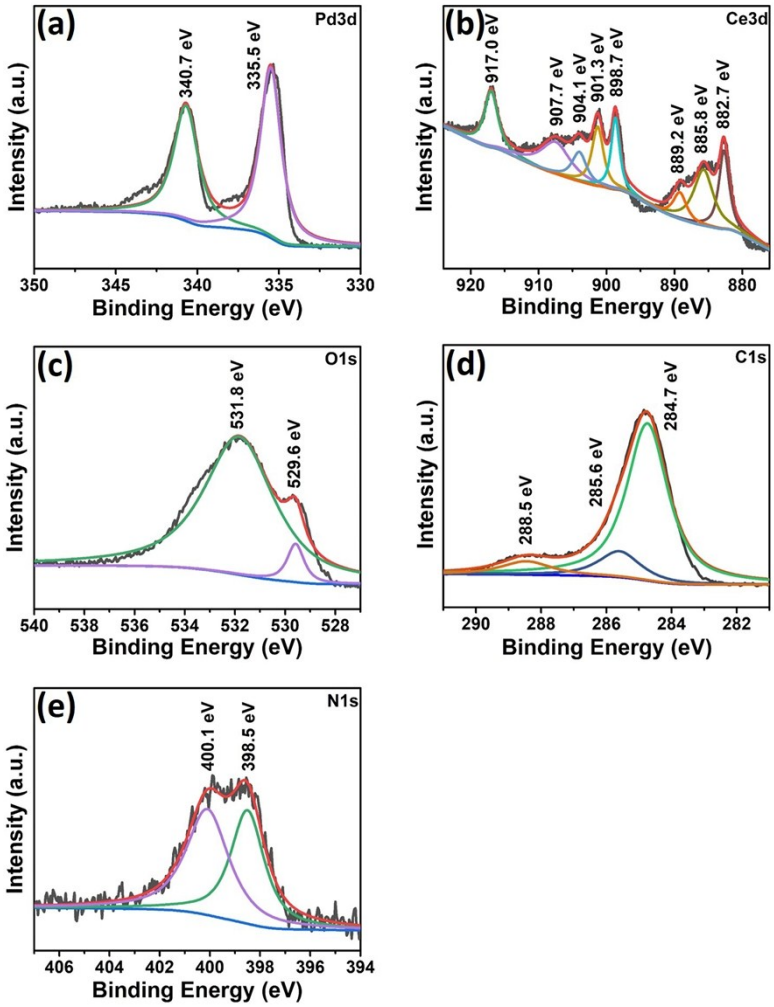

Fig. S8 XPS spectra of (a) Pd 3d, (b) Ce 3d, (c) O 1s, (d) C 1s and (e) N 1s for Pd/CeO_2@NC-600.

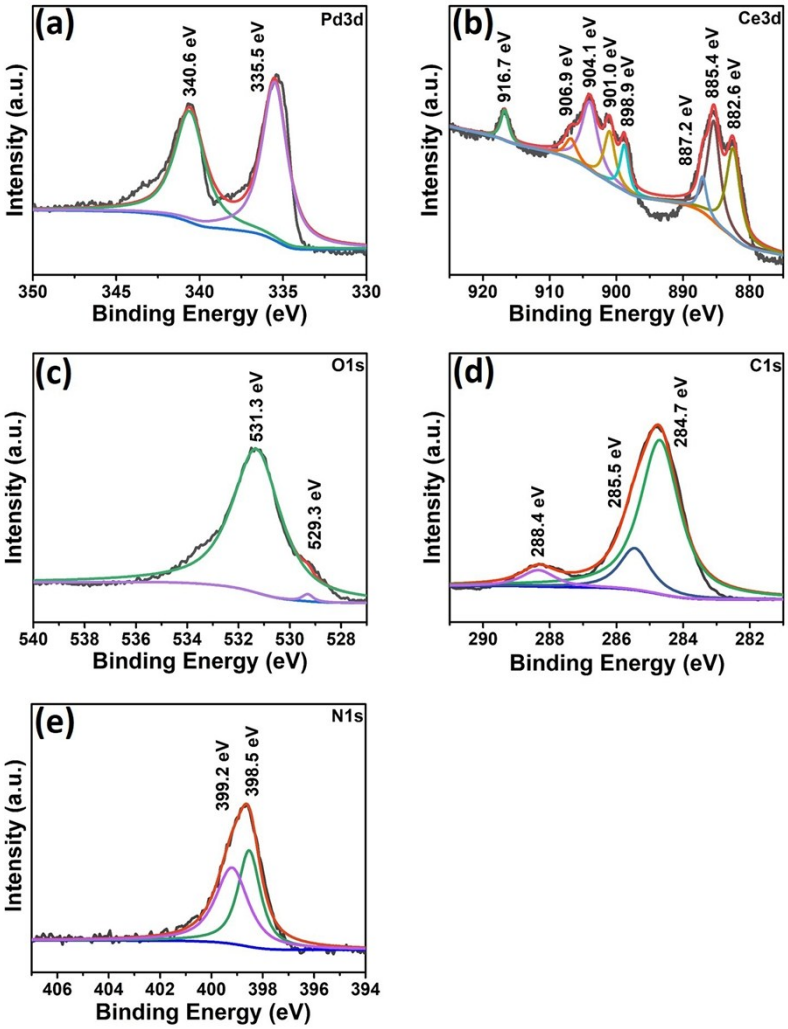

Fig. S9 XPS spectra of (a) Pd 3d, (b) Ce 3d, (c) O 1s, (d) C 1s and (e) N 1s for Pd/CeO_2@NC-800.

9. ICP characterization of Pd/CeO_2@NC-700

The Pd and Ce contents were determined by inductively coupled plasma atomic emission spectroscopy (ICP-AES) on an IRIS Intrepid II XSP instrument (Thermo Electron Corp.) and the results are summerized in Table S3.

Table S3. ICP results of Pd/CeO_2@NC-700.

Act Wgt/g	Act Vol/ml	DF	Element	Soln Conc	Units	Corr Con	Units
0.0052	25	1	Ce	16.809	mg/L	80813.5	mg/kg
0.0052	25	100	Pd	0.7014	mg/L	337192.3	mg/kg

10. Catalytic studies on CO Oxidation of Pd/CeO_2@NC-700

The TEM images of Pd/CeO_2@NC-700 after stability test are shown in Fig. S10. As revealed, the Pd and CeO_2 NPs are still highly dispersed (Fig. S10a) and closely connected (Fig. S10b) as in the original sample, and no reduction of the crystallinity of Pd and CeO_2 NPs has been found (Fig. S10c and 10d).

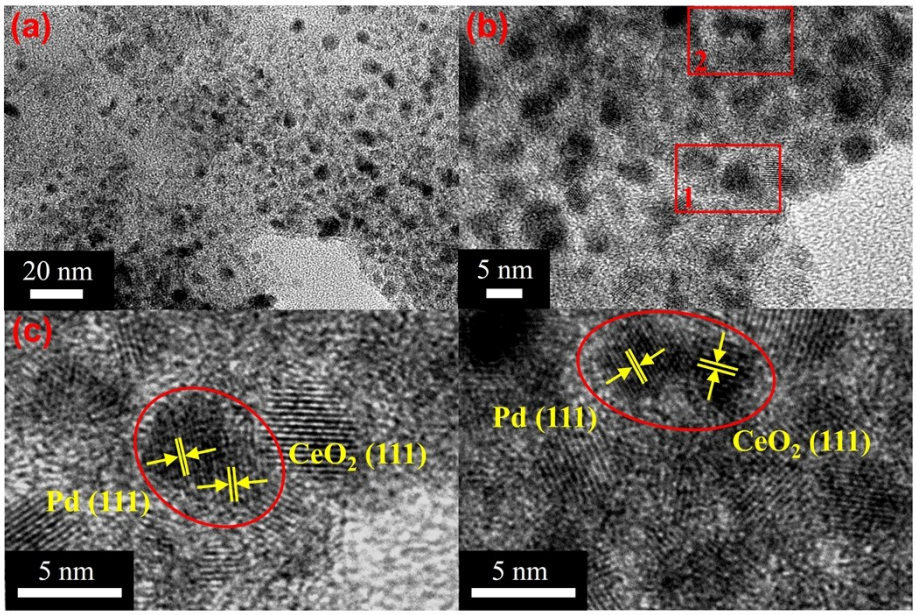

Fig. S10 TEM images of Pd/CeO_2@NC-700 after stability test.